Enhanced Dielectric Relaxation in Self-Organized Layers of Polypeptides Coupled to Platinum Nanoparticles: Temperature Dependence and Effect of Bias Voltage

Louis Merle, Ghada Manai, Adeline Pham, Sébastien Lecommandoux, Philippe Demont, Colin Bonduelle, Simon Tricard, Adnen Mlayah, Jérémie Grisolia

Enhanced Dielectric Relaxation in Self-Organized Layers of Polypeptides Coupled to Platinum Nanoparticles: Temperature Dependence and Effect of Bias Voltage

Louis Merle[1], Ghada Manai[1], Adeline Pham[1], Sébastien Lecommandoux[2], Philippe Demont[3], Colin Bonduelle[2], Simon Tricard[1], Adnen Mlayah[4,5], Jérémie Grisolia[*1]

[1] LPCNO, Université de Toulouse, INSA, CNRS, UPS, 135 Avenue de Rangueil, Toulouse 31077, France

[2] LCPO, Université de Bordeaux, CNRS, Bordeaux INP, LCPO UMR 5629, F-33600 Pessac, France

[3] CIRIMAT, Université Toulouse - Paul Sabatier, 118 Route de Narbonne 31062 Toulouse, France

[4] CEMES, Université de Toulouse, CEMES-CNRS, 29 rue Jeanne Marvig, Toulouse 31055, France

[5] LAAS, Université de Toulouse, CNRS, UPS, Toulouse, France

* Corresponding author: jeremie.grisolia@insa-toulouse.fr

Abstract

Using alternative current impedance spectroscopy, we investigate the dynamical conductivity of hybrid nanomaterials composed of helical polypeptide layers containing platinum nanoparticles. The electrical characteristics of the self-organize poly(γ-benzyl-*L*-glutamate) (PBGL) in bidimensional lamellar assembly in the presence of Pt nanoparticles are well modelled and described by a single equivalent circuit of parallel resistance and capacitance. The latter are determined using a comparison between the measured and calculated Nyquist plots, which allows extracting the characteristic relaxation time and frequency of the dipolar relaxation process. We found that the relaxation frequency in the PBLG-PtNP hybrid materials is enhanced by four orders of magnitudes compared to pure PBLG, which indicates a much faster dielectric relaxation in PBLG-PtNP due to dipole orientation and dipole-dipole interactions. The temperature dependence of the relaxation time is analyzed using Arrhenius plots, from which the activation energy of the relaxation process is found to be around 0.1 eV. Such a value close to the peptide vibration energy of the PBLG, indicates a vibrational assisted relaxation process and a polaronic charge transport mechanism. An advantage of the PBLG-PtNP nano-composite material is that the activation energy can be finely tuned by the PBLG degree of polymerization. Finally, an important outcome of this work is the investigation of the dielectric relaxation process in PBLG-PtNP under applied DC bias. We found that the activation energy decreases with increasing bias voltage for

all degrees of polymerization of the PBLG molecule. This effect is interpreted in terms of electric field induced alignment of the dipoles and of increased mobility of the polaronic charge carriers. The presence of piezo-electricity in the hybrid material gives the possibility to use the DC bias as a simple mean of monitoring the dynamical conductivity involving polaronic states.

Introduction:

Nanocomposites are defined here as hybrid materials where both organic and inorganic phases coexist, and exhibit a spatial organization at the nanoscale. These two phases present complementary properties (magnetic, electronic, photonic) (1] generated by a synergy between the different species. These novel materials are very promising for applications in strain sensors [2], or memories [3], and more generally in nanoelectronics [4-5]. In addition to the nature of the components of the hybrid material, the structural organization – at the nanoscale – brings out new mechanical [6] and electrical properties [7]. A recent strategy to provide nanocomposites is to co-assemble peptidic polymers and metallic nanoparticles [8]. Indeed, polypeptide polymers present an ordered secondary structure in α helix, in β sheet or a disordered structure in random coil [9], each conformation having its intrinsic properties (hydrodynamic volume, rigidity, solubility, Van der Walls bonding) [9-11], and is responsible for structural organization up to the macroscopic scale [12]. A particularity of α helical polypeptides is the existence of a piezoelectric character [13] if the electric dipoles are parallel to the helix axis. In the case of Pt nanoparticles (NP) and poly(γ-benzyl-*L*-glutamate) (PBLG) in α helix, the system presents a lamellar organization of the PBLG molecules [8]. In such a system, the α helices aligned with each other to form lamellae separated by lines of nanoparticles, the surface of which interacts with functional groups of the PBLG by coordination interactions. The multi-scale characteristics of these nanocomposites, composed of conductive and insulating domains, strongly impact their dielectric properties such as dipolar relaxation and dynamical conductivity which can be finely probed using AC impedance spectroscopy. It is therefore interesting to investigate the dynamical transport mechanisms in these systems for fundamental understanding of the correlation between electrical transport and piezo-electric properties and the structural organization of the hybrid Pt/PBLG material.

In this work, we focus on the dielectric response of different hybrid material composed of PBLG in α helix conformation and Pt NP using AC impedance spectroscopy [14]. Impedance spectroscopy allows the understanding of the transport and relaxation mechanisms that take place in the material, through the activation energy of the process. The activation energy of the relaxation process responsible for the dynamical conductivity depends on the materials and on the nature of the conduction processes. It can range from tens of meV in the case of Pd-ZrO_2 [15-16] to several hundreds of meV in hybrid polymer systems, such as polyvinyl alcohol containing barium zirconium titanate ceramic [17]. The measured impedance spectra are interpreted using equivalent electrical circuits combining the PBLG-PtNP resistance and capacitance as well as the contact electrode resistance. The studied system PBLG-PtNP can then be considered as a granular system composed of insulating and conducting phases. The temperature dependence of the so-extracted relaxation time allows determining the activation energy. In the present work, we focus on the activation energy of the relaxation process responsible for the dynamical conductivity of the PBLG-PtNP layers. In particular, we investigate the change of the activation energy with the degree of polymerization of the PBLG molecules, and its relation on an applied DC bias voltage.

Methods

Platinum nanoparticles of 1.2 ± 0.3 nm in diameter were synthesized by decomposition of Pt_2(dba) in tetrahydrofuran (THF) under an atmosphere of CO, followed by complete elimination of the organic dibenzylideneacetone (dba) residue by washing with pentane [18]. Poly(γ-benzyl-*L*-glutamate) (PBLG) was obtained by ring-opening polymerization of γ-benzyl-*L*-glutamate *N*-carboxyanhydride monomers using propargylamine as initiator in dimethylformamide [19]. The polymerization degree (DP) of the PBLG was controlled during the synthesis by adjusting the stoichiometry of the initiator (I) as compared to the monomer (M; M/I ratio or theoretical DP). With theoretical DP of 60, 120, 240 and 480, the labelled samples PBLG1, PBLG2, PBLG3 and PBLG4 have respectively the following DP: 69, 120, 217 and 481. The hybrid PBLG-PtNP composite is obtained by mixing the Pt nanoparticles with PBLG in THF. Solutions of PtNPs and of PBLG were mixed and stirred for 2h at an equivalent number of 0.5 (equivalent number is the ratio between the monomer unit and the Pt atom quantities), as the

assembly process occurs at an optimum relative ratio of polymer vs. nanoparticle equals to 0.5 eq [*8*]. The PBLG-PtNP composite formed bi-dimensional layers already present in solution [*8*].

Pure PBGL and PBLG-PtNP were tested using a T-shaped architecture with two copper pads connected to inter-digitated 250 × 100 × 0.1 µm comb electrodes separated by 5 µm [*20*]. Electric characteristics were measured using a Janis ST-500-1 cryogenic probe station. The sample temperature was monitored in the 290-350K range using a Lakeshore 350 controller operating at 2K/min heating rate. Impedance spectroscopy measurements were performed, using a Keysight Impedance Analyzer EA4990A, in the 20Hz-5MHz frequency range with a 500mV AC voltage and under applied bias voltage ranging from 0V to 2.5V.

Results and discussion:

Degree of polymerization (DP)

Figure 1a-d display TEM (Transmission Electron Microscopy) images of the hybrid PBLG-PtNP material obtained with the different polymerization degrees of PBLG. The regions of high and low densities of Pt NPs in PBLG are visible in Figure 1a-d as alternated dark and bright areas, respectively. As shown in a previous work [8], the size of PBLG areas, with low density of Pt NPs, increases with increasing DP as $d = 0.095 \times DP$.

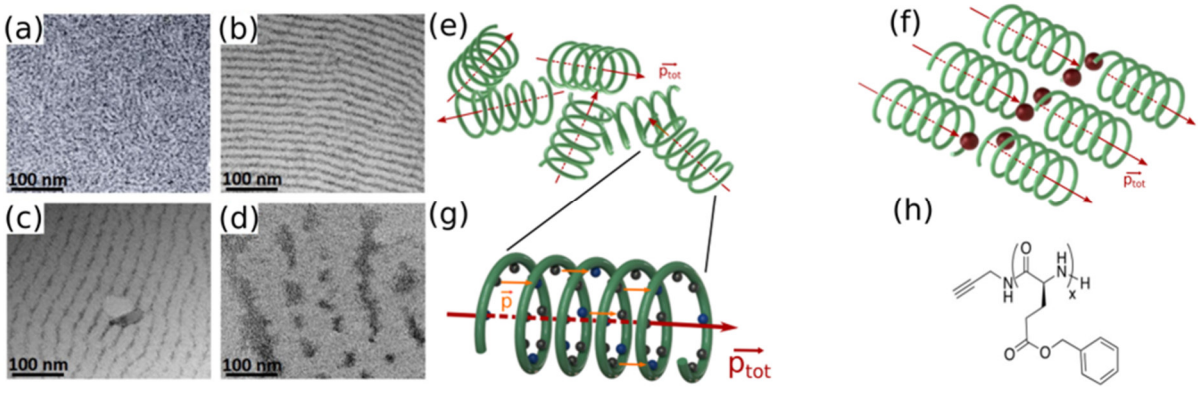

Figure 1 : a-d TEM images of PBLG-PtNP for different polymerization degrees (DP): (a) PBLG1 (DP 69), (b) PBLG2 (DP120), (c) PBLG3 (DP 217), (d) PBLG4 (DP 481). Regions of high density of Pt NPs appear as dark regions contain NPs whereas the regions of pure PBLG appear bright. Schematic of the helical structure of PBLG

without Pt NP (e), and in the presence of Pt (f). PBLG is represented in green and the Pt NP in red spheres. (g) Schematic representation of an α helix PBLG molecule, orange arrows describe the resulting electrical dipole moments carried by the peptide bond. The red arrows represent the total electrical dipole moment carried by the chain. (h) Cram representation of PBLG with x the polymerization degree (DP).

One can notice that the organization of the PBLG-PtNP composite film evolves with DP from a short range (sub-10 nm) ordered structure (PBLG1) to a periodic alternation of dark and bright regions of Pt NPs rich and Pt NPs free region of PBLG, particularly for PBLG2 and PBLG3. Indeed, a characteristic feature of PBLG-PtNP is its lamellar structural organization at a mesoscopic scale [*δ*] (Figure 1b-d and f), which arises from areas of well aligned PLBG chains, with a α helix structure [21] (Figure 1g) bridged by areas containing Pt NPs and PBLG in random coil. On the contrary, the pure PBLG film exhibits no organization (Figure 1e). The presence of Pt NPs leads to the lamellar structure of the PBLG-PtNP composite with optimum DP of 120 and 217 (respectively PBLG2 and PBLG3) (Figure 1b and c, Figure SI 1). For PBLG4, the Pt NPs agglomerate in rather large (sub 100 nm) and isolated paquets which results in a less ordered, but still aligned, structure (Figure 1d).

Monomer units of the PBLG carry a resulting electrical dipole on the peptide bonds of the α helix. The repetition of monomer units, in helical conformation, results in a large electrical dipole and hence the PBLG acquires piezo-electric properties [13]. However, the dipole orientation is random in the disordered phase (PBLG without Pt NPs, Figure 1e) and the average macro-dipole cancel out. Whereas in the ordered phase (Figure 1f), due to the lamellar structure of the composite PBLG-PtNP film, the dipoles attached to each α helix PBLG chain are aligned and sum up, thus giving rise to a macro-dipole at a macroscopic scale. Piezo-electricity may thus emerge as a result of the lamellar self-organisation of the composite PBLG-PtNP material. Moreover, the PBLG-PtNP composite material is a granular system with insulating (PLBG) and conducting (Pt-NP) components, the electrical transport properties of which can be fully characterized using impedance spectroscopy [15].

Figure 2 shows room-temperature impedance spectra acquired in the 20 Hz to 5 MHz frequency range with 500 mV AC voltage and 0V DC bias. Figure 2a presents the Nyquist impedance plots of PBLG-PtNP for the investigated DP values:

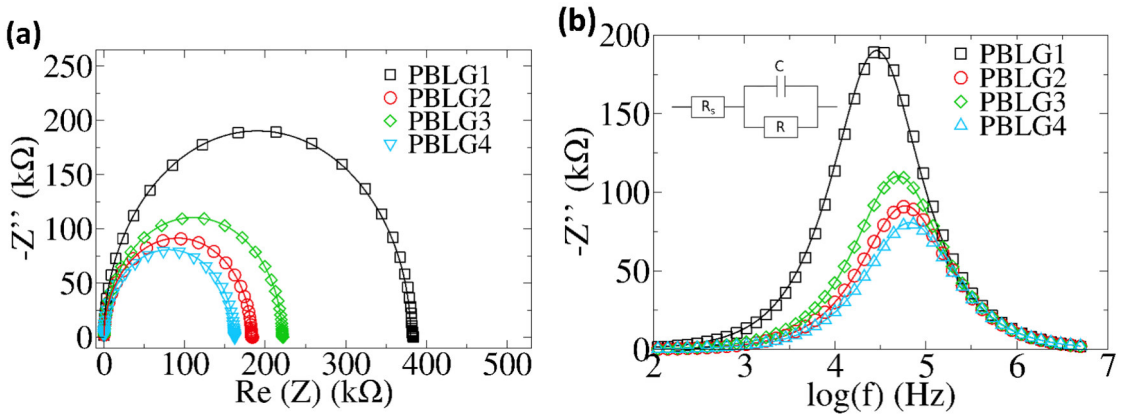

Figure 2 : Experimental (symbols) Nyquist's impedance plots (i.e. Z' vs -Z'' in kΩ) of PBLG-PtNP and fit (straight lines) for PBLG1, PBLG2, PBLG3, PBLG4. (b) -Z'' as a function of frequency with experimental data (symbols) and Lorentzian fit (straight lines). The electrical equivalent circuit used for the modeling of the frequency dependent impedance is shown in the inset.

Each sample exhibits semi-circle whose radius gives the impedance modulus, which is in the order of hundreds of kΩ. A remarkable point is that whatever the DP, the impedance-of the PBLG-PtNP layers is four orders of magnitude smaller than the one measured on a pure PBLG layer (*i.e.* without Pt NPs) which is around several GΩ (supplementary information Figure SI 2). These measurements clearly indicate the self-assembly created by the synergy of PBLG and Pt NPs strongly enhance the dynamical conductivity of the composite material reducing its electrical impedance by four orders of magnitudes. PBLG1 exhibits the lowest degree of organisation (Figure 1) and has the largest impedance (around 400 kΩ at low frequency), as shown in Figure 2a. The impedance of the more ordered layers (PBLG2 to 4) is reduced by roughly a factor of two compared to PBLG1 (Figure 2a). However, the impedance measured for PBLG3 (225 kΩ) is larger than the one measured for PBLG2 (175 kΩ). This inversion of conductivity is attributed to structural defects in the organisation of the layer. Indeed, the disorder in the lamellar organization, *i.e.* variations in orientations of the lamellae separated by grain boundaries and defects in their contact to the electrodes, may reduce the conductivity of the layer and explain the non-monotonic evolution of the Nyquist plots with the degree of polymerization (Figure 2a).

Figure 2b shows spectra of the imaginary part Z'' of the impedance as a function of frequency measured for the PBLG-PtNP layers. Firstly, each spectrum consists of a single Lorentzian-like resonance peak, as confirmed by the plot of the electrical modulus versus log(f) (see Figure SI 3), indicating a single electrical relaxation phenomenon responsible for the dynamical conductivity

response of the composite layers. It is characterized by well-defined resonance frequency f_c and relaxation time τ. A f_c= 30 kHz corresponds to τ = 33 µs is found for PBLG1. For all other samples, from PBLG2 to 4, the resonance frequency increases with respect to PBLG1 and reaches f_c= 65 kHz (τ =15 µs) for PBLG4. One can notice that PBLG3 exhibits a fc= 60 kHz which is slightly higher than that observed fc=50 kHz for PBLG2, which confirms that not only the DP but also the ordering of the layer may impact the relaxation dynamics, as already noticed in Nyquist plots (Figure 2a).

It is worth mentioning that the resonance frequencies observed here for the PBLG-PtNP composite layers are much larger (at least four orders of magnitudes) than the one estimated for pure PBLG (supplementary information Figure SI 2). This difference indicates that the ordering of the PBLG molecules in the PBLG-PtNP composite material strongly impacts not only the magnitude (Figure 2a) of the electrical impedance but also the relaxation dynamics (Figure 2b) of the dipoles carried by each PBLG molecule (Figure 1g). Indeed, we suggest that the ordering of the PBLG molecules in the lamellar structure (Figure 1f) leads to dipoles alignment and to efficient dipole-dipole interaction, and hence to a blockade of the reorientation of the dipoles. As a consequence, the relaxation process of the interacting dipoles occurs at a much higher frequency, compared to the case of randomly oriented PBLG molecules (*i.e.*, pure PBLG) thus reflecting the structural ordering of the PBLG molecules in the PBLG-PtNP composite material.

The semi-circular shape of Nyquist plots (Figure 2a) indicates that the electrical conductivity of the PBLG-PtNP layers can be-modelled using an electrical equivalent circuit consisting of a parallel resistance R and capacitance C [*15*]. An additional series resistance R_s is included to account for the electrode's resistance. The complex impedance of the equivalent electrical circuit is then defined as:

$$Z(\omega) = Z'(\omega) + jZ''(\omega) = R_S + \frac{R}{1+jRC\omega} \quad (1)$$

where Z' and $Z''$are, respectively, the real and imaginary part of the impedance at angular frequency ω, R, C and R_S. These latter values being determined using a lest-square fit of the calculated impedance (Eq (1)) to the measured one. The relaxation time is hence obtained as $\tau = RC = \frac{1}{2\pi f_c}$.

Temperature effect

Figure 3a displays temperature dependent Nyquist plots for the PBLG2 composite with no applied DC bias. The samples PBLG1, PBLG3, PBLG4 exhibit a similar behavior: the radius of the semi-circles, and the total impedance of the sample, decrease with increasing temperature.

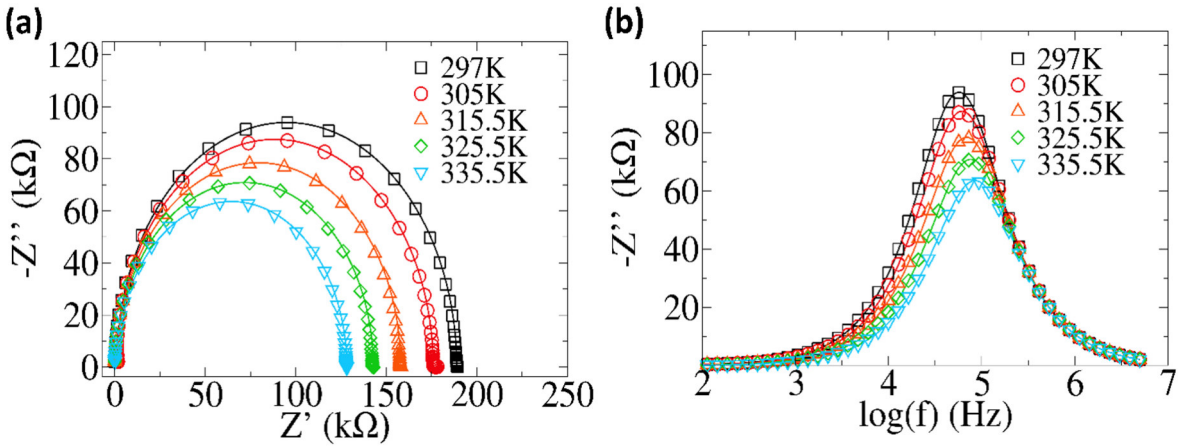

Figure 3 : (a) Experimental (symbols) Nyquist's impedance plots (Z in kΩ) of PBLG2 and fit (straight lines) for temperatures between 297K and 335.5K. (b) -Z'' as a function of frequency with experimental data (symbols) and fit (straight lines) for various temperature.

This is corroborated by the temperature dependence of the resistance R and capacitance C (see supplementary Figure SI 4). These latter values were extracted from Nyquist plots using a fitting procedure based on equation *(1)*. We found that the resistance decreases by 0.8 %/K whereas the capacitance decreases by only 4.10^{-3} %/K with increasing temperature. This observation indicates that the temperature dependence of the impedance is mainly due to its resistive component and that the relaxation process is thermally activated. Correlatively, the impedance resonance peak shifts towards higher frequencies with increasing temperature (Figure 3b), which reveals that the relaxation process at work is getting faster thus confirming its thermally activated nature. Indeed, because of its lamellar structure, PBLG-PtNP presents a dielectric component, the resistance of which may decrease with increasing temperature due to thermally enhanced carrier mobility [22]. Such an enhancement can occurs in several charge transport mechanisms involving hopping between trapping sites, quantum tunneling and formation of large polarons [*23-25*].

The change of the resonance peak frequency f_c as a function of temperature extracted from the spectra in Figure 3b allows the determination of the activation energy of the relaxation phenomenon,

responsible for the dynamical conductivity of our composite PBLG-PtNP nanomaterials. Assuming that f_c follows an Arrhenius law [*17*], its temperature dependence is given by

$$f_c = f_0 e^{\frac{-E_a}{kT}} \quad (2)$$

where f_0 is the resonance frequency at high temperature, k is the Boltzmann constant, and E_a the activation energy. As shown by the Arrhenius plots (Figure 4) the temperature dependence f_c is well described using a single activation energy, which confirms that a single conduction mechanism can account for the experimental data.

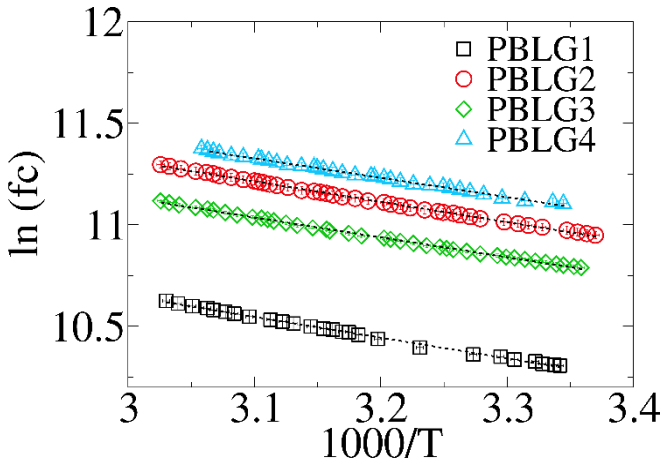

Figure 4 : ln (fc) as a function of 1000/T for PBLG1, PBLG2, PBLG3, PBLG4.at 0 DC bias voltage. Symbols represent experimental data and lines are linear fits.

This single conduction mechanism is in contrast to the one pointed out in composite materials involving polydispersed nanoparticles [26] or particles of several micrometers in size [27], where two activation energies are generally found; one is associated with the grains themselves and the other one with the grain boundary. In our samples the nanometer size of the Pt NPs (1.2 nm) leads to a grain capacitance of a few fF only [*20*] and therefore to relaxation frequencies of NPs above 5MHz. Grain effects are thus negligible here. Only the activation energy of dielectric relaxation process involving the PBLG is thus measurable in our frequency range. The activations energies extracted for the PBLG-PtNP samples with PBLG1-4 are respectively 0.102 eV, 0.105 eV, 0.098eV and 0.095eV (± 0.001 eV). These values lie in the 900-1000 cm^{-1} range, *i.e.* close to the vibration frequency of the stretching mode of the CN bond (*c.a.* 1200 cm^{-1}, *i.e.* 0.15 eV) [*8*]. The fact that the obtained activation energies are close to that of the

peptide group vibrations strongly suggests a thermally activated dipole relaxation process. The relaxation rate is therefore expected to be proportional to the thermal population of vibration modes of the peptide group which is given by the Bose-Einstein factor. The latter can be approximated by $exp\left(\frac{-\hbar\omega}{kT}\right)$ in the considered temperature range. Comparison with Arrhenius law (Eq. (2)) strongly suggests that the relaxation frequency is indeed proportional to the thermal population of the peptide vibrations and that the relaxation process and the dynamical conductivity are assisted by such vibrations in our PBLG-PtNP nanomaterials.

DC bias voltage effect

The piezo-electric properties of the synthesized PBLG-PtNP nanomaterials were investigated by impedance spectroscopy measurements under various applied DC bias voltages. Figure 5 shows typical experimental results (here displayed only for the PBLG2). Both Nyquist plots (Figure 5a) and –Z'' impedance spectra (Figure 5b) are displayed.

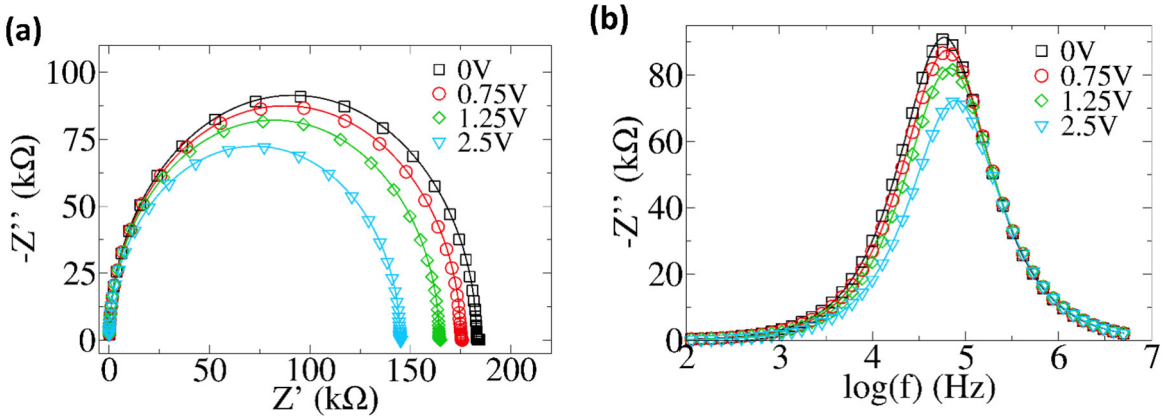

Figure 5 : (a) Room-temperature experimental (symbols) Nyquist's impedance plots (Z in kΩ) of PBLG-PtNP with PBLG2 and fitted (Eq (1)*) plots (lines) for DC bias voltage ranging from 0V to 2.5V under 300K. (b) Room temperature measured spectra of -Z'' as a function of frequency with spectra experimental data (symbols) and corresponding fits (straight lines) for DC bias voltage ranging from 0V to 2.5V.*

The impedance decreases with increasing DC bias voltage (Figure 5a) following a linear variation with a characteristic slope of -10 kΩ/V. Moreover, the resonance frequency of the impedance peak (Figure 5b) increases linearly by 7.6 kHz/V with increasing bias voltage. All investigated hybrid PBLG-PtNP nanomaterials exhibit a similar behavior with respect to the applied bias voltage. It is worthwhile to mention that the sensitivity of PBLG-PtNP to an applied external electric field is not

observed in the pure PBLG reference sample (Figure SI 5), *i.e.* without Pt nanoparticles. The dependence to the DC bias is explained by the lamellar structure of PBLG-PtNP (Figure 1f) which favors the alignment of the microscopic dipoles and thus the emergence of a macroscopic polarization (Figure 1) that can be modulated by an applied external field. No such macroscopic polarization is present in the pure PBLG sample. To go deeper into the understanding of the effect of the applied field on the transport properties and relaxation dynamics, we have performed temperature dependent impedance spectroscopy measurements under applied DC bias voltage.

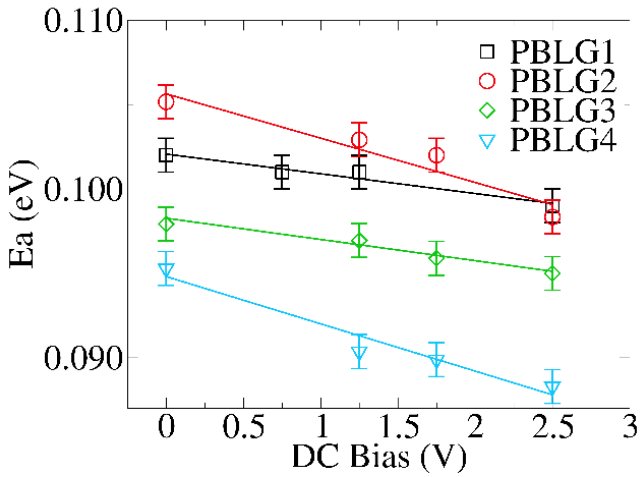

Figure 6 : Activation energy (± 0.001 eV) versus DC bias voltage (V) extracted from Arrhenius law. To each type of symbol is associated extracted activation energies of PBLG1-4 and corresponding fit (straight lines).

In this way, we are able to extract the dependence of the activation energy (Eq. (2), Figure SI 6) on the applied bias voltage. The so-obtained results are presented in Table 1:

	Activation Energy (eV)			
DC Bias (V)	*PBLG1*	*PBLG2*	*PBLG3*	*PBLG4*
0	0.102	0.105	0.098	0.095
0.75	0.101	-	-	-
1.25	0.101	0.103	0.097	0.090
1.75	-	0.102	0.096	0.089
2.5	0.099	0.098	0.095	0.088
	$dEa/dU\ (eV.V^{-1})$			
	PBLG1	*PBLG2*	*PBLG3*	*PBLG4*
	−0.012	−0.026	−0.013	−0.028

Table 1 : Activation energy of PBLG1-4 and the derivative of the activation energy with DC bias voltage.

At zero DC bias, the measured activation energy is of the order of 0.1 eV for all DPs and decreases almost linearly with increasing bias voltage with characteristic slopes between -0.012 eV/V (for PBLG1) and -0.028 eV/V (for PBLG4).

The drop of the activation energy with applied DC bias is interpreted in terms of orientation of the dipoles, carried by the PBLG molecules, along the direction of the imposed DC electric field. The electric field induced alignment of the dipoles may in turn decrease the energy barrier of the localized polarons thus leading to an increased carrier mobility and a lowering of the impedance as observed in Figure 5a. One can notice that, for PBLG3 and-PBLG4, the activation energy decreases by only 0.001eV, for DC bias increasing from 1.75V to 2.5V, which suggests a possible saturation of the effect corresponding to a full alignment of the dipoles with the applied DC electric field. Such an effect could be related to the spatial distribution of the PBLG molecules in the lamellar structure with several orientation domains separated by grain boundaries.

Conclusion

In summary, we have investigated the dynamical conductivity of a polypeptide-nanoparticle nanocomposite using impedance spectroscopy measurements. The lamellar organization of PBLG with Pt NPs provides electrical dipole moments at the scale of the polymer chains. The increase of the PBLG relaxation frequency by four orders of magnitudes in the presence of Pt NP underlines the importance of the supramolecular organization. Such an organization facilitates the orientation and alignment of the dipoles, with activation energies of the order of 0.1 eV, comparable to the ones reported for hybrid granular materials. Besides, high polymerization degree of the PBLG molecules favors the lamellar organization and the emergence of coherent polarization domains. Indeed, the higher the molar mass of the polymer, the higher the dipole moment of the chains, the lower the nanocomposite activation energy. The application of a DC bias voltage also decreases the activation energy, by orienting the electric dipoles along the applied field. Self-assembly of hybrid materials is a fundamental approach to synthesize nanocomposites, with physical responses comparable to the ones of inorganic compounds, but with the flexibility afforded by the polymer and nanoparticle chemistries. The presented work unravels the impact of the organization of the PBLG-PtNP hybrid material on its electrical parameters, which is useful for the development of novel devices in nanoelectronics.

Supporting Information.

TEM images of PBLG-PtNP, Nyquist plot of unstructured PBLG2, Imaginary part of the electrical modulus M as a function of frequency in a semi-log scale, capacitance and resistance measured as a function of temperature, Nyquist plot of unstructured PBLG2 for DC bias voltage between 0V and 2.5V, Arrhenius plots of the resonance peak frequency fc for DC bias voltage between 0V and 2.5V, and for (a) PBLG1, (b) PBLG2, (c) PBLG3, (d) PBLG4.

Acknowledgment

The authors thank S. Raffy and C. Midelet for fruitful discussions on the support of fitting and graphing. Financial support from Université de Toulouse (NaSAPeP grant APR), from CNRS (MITI interdisciplinary programs, COCOPIE project) and from Agence Nationale de la Recherche (MOSC grant ANR-18-CE09-0007) is acknowledged. This study has been partially supported through the EUR

grant NanoX n°ANR-17-EURE-0009 in the framework of the Programme des Investissements d'Avenir.

References

(1) Kao, J.; Thorkelsson, K.; Bai, P.; Rancatore, B. J.; Xu, T. Toward functional nanocomposites: taking the best of nanoparticles, polymers, and small molecules. *Chem Soc Rev* **2013**, vol. 42, no 7, p. 2654 2678 doi: 10.1039/C2CS35375J.

(2) Kim, Y.-J.; Cha, J. Y.; Ham, H.; Huh, H.; So, D.-S.; Kang, I.. Preparation of piezoresistive nano smart hybrid material based on graphene , Curr. *Appl. Phys.* **2011** vol. 11, nº 1, p. S350-S352 doi: 10.1016/j.cap.2010.11.022.

(3) Verbakel, F.; Meskers, S. C. J.; Janssen, R. A. J. Electronic memory effects in diodes from a zinc oxide nanoparticle-polystyrene hybrid material. *Appl. Phys. Lett.* **2006,** vol. 89, nº 10, p. 102103, doi: 10.1063/1.2345612.

(4) Huynh, W. U. Hybrid Nanorod-Polymer Solar Cells. *Science* **2002**, vol. 295, nº 5564, p. 2425-2427, doi: 10.1126/science.1069156.

(5) Balazs, A. C.; Emrick, T.; Russell, T. P. Nanoparticle Polymer Composites: Where Two Small Worlds Meet. *Science* **2006**, vol. 314, nº 5802, p. 1107-1110, doi: 10.1126/science.1130557.

(6) Crosby, A. J.; Lee, J. Polymer Nanocomposites: The "Nano" Effect on Mechanical Properties. *Polym. Rev.* **2007,** vol. 47, nº 2, p. 217-229, doi: 10.1080/15583720701271278.

(7) Yi, C.; Yang, Y.; Liu, B.; He, J.; Nie, Z. Polymer-guided assembly of inorganic nanoparticles. *Chem. Soc. Rev.* **2020** , vol. 49, nº 2, p. 465-508, doi: 10.1039/C9CS00725C.

(8) Manai, G. et al. Bidimensional lamellar assembly by coordination of peptidic homopolymers to platinum nanoparticles. *Nature Communications* **2020**, volume 11, Article number: 2051.

(9) Bonduelle, C. Secondary structures of synthetic polypeptide polymers. *Polym. Chem.* **2018**, vol. 9, nº 13, p. 1517-1529, doi: 10.1039/C7PY01725A.

(10) Sharp, M. Dielectric Study of Dilute Solutions of Poly-y-benzyl-L-glutamate. *J Chem SOC* **1970**, p. 1596-1601.

(11) Kratzmüller, T.; Appelhans, D.; Braun, H.-G. Ultrathin Microstructured Polypeptide Layers by Surface-initiated Polymerization on Microprinted Surfaces. *Adv. Mater.* **1999**, vol. 11, nº 7, p. 555-558.

(12) Cai, C.; Lin, J.; Lu, Y.; Zhang, Q.; Wang, L. Polypeptide self-assemblies: nanostructures and bioapplications. *Chem. Soc. Rev.* **2016**, vol. 45, nº 21, p. 5985-6012, doi: 10.1039/C6CS00013D.

(13) Jaworek, T.; Neher, D.; Wegner, G.; Wieringa, R. H.; Schouten, A. J. Electromechanical Properties of an Ultrathin Layer of Directionally Aligned Helical Polypeptides. *Science* **1998**, vol. 279, p. 57-62.

(14) Kuwabara, T.; Kawahara, Y.; Yamaguchi, T.; Takahashi, K. Characterization of Inverted-Type Organic Solar Cells with a ZnO Layer as the Electron Collection Electrode by ac Impedance Spectroscopy. *ACS Appl. Mater. Interfaces* **2009**, vol. 1, nº 10, p. 2107-2110, doi: 10.1021/am900446x.

(15) Bakkali, H.; Dominguez, M.; Batlle, X.; Labarta, A. Universality of the electrical transport in granular metals, *Sci. Rep.* **2016**, vol. 6, nº 1, p. 29676, doi: 10.1038/srep29676.

(16) Bakkali, H.; Dominguez, M.; Batlle, X.; Labarta, Equivalent circuit modeling of the ac response of Pd-ZrO2 granular metal thin films using impedance spectroscopy. *Journal of Physics D Applied Physics* **2015**, Volume 48, Number 33, 5306.

(17) Senthil, V.; Badapanda, T.; Kumar, S. N.; Kumar, P.; Panigrahi, S. Relaxation and conduction mechanism of PVA: BYZT polymer composites by impedance spectroscopy. *J. Polym. Res.* **2012**, vol. 19, nº 3, p. 9838, doi: 10.1007/s10965-012-9838-0.

(18) Tricard S. et al. Chemical tuning of Coulomb blockade at room-temperature in ultra-small platinum nanoparticle self-assemblies. *Mater. Horiz.* **2017**, vol. 4, nº 3, p. 487-492, doi: 10.1039/c6mh00419a.

(19) Schatz, C.; Louguet, S.; Meins, J.-F. L.; Lecommandoux, S. Polysaccharide-block-polypeptide Copolymer Vesicles: Towards Synthetic Viral Capsids. *Angew Chem Int Ed* **2009**, vol. 48, p. 2572-2575.

(20) Nesser, H.; Grisolia, J.; Alnasser, T.; Viallet, B.; Ressier, L. Towards wireless highly sensitive capacitive strain sensors based on gold colloidal nanoparticles. *Nanoscale* **2018**, vol. 10, nº 22, p. 10479-10487, doi: 10.1039/C7NR09685B.

(21) Chang, Y. C.; Frank, C. W.; Forstmann, G. G.; Johannsmann, D. Quadrupolar and polar anisotropy in end-grafted α-helical poly(γ-benzyl- L -glutamate) on solid substrates. *J. Chem. Phys.* **1999**, vol. 111, nº 13, p. 6136-6143, doi: 10.1063/1.479909.

(22) Saha, T. K.; Purkait, P. Investigations of Temperature Effects on the Dielectric Response Measurements of Transformer Oil-Paper Insulation System. *IEEE Trans. Power Deliv.* **2008**, vol. 23, nº 1, 252-260, doi: 10.1109/TPWRD.2007.911123.

(23) Coşkun, M.; Polat, O.; Coşkun, F.M.; Durmuş, C.; Çağlard, M.; Türüt A. Frequency and temperature dependent electrical and dielectric properties of LaCrO 3 and Ir doped LaCrO 3 perovskite compounds. *Journal of Alloys and Compounds* **2018,** 740, 1012-1023.

(24) S. Nasri; M. Megdiche; M. Gargouri. DC conductivity and study of AC electrical conduction mechanisms by non-overlapping small polaron tunneling model in LiFeP2O7 ceramic. *Ceram. Int.* **2016**, vol. 42, nº 1, p. 943-951, doi: 10.1016/j.ceramint.2015.09.023.

(25) Morita, T.; Kimura, S. Long-Range Electron Transfer over 4 nm Governed by an Inelastic Hopping Mechanism in Self-Assembled Monolayers of Helical Peptides. *J. Am. Chem. Soc.* **2003**, vol. 125, nº 29, 8732-8733, doi: 10.1021/ja034872n.

(26) Bakkali, H.; Dominguez, M. Differential conductance of Pd-ZrO2 thin granular films prepared by RF magnetron sputtering. *EPL* **2013**, 104, 1, 17007.

(27) Coşkun, M.; Polat, O.; Coşkun, F.M.; Durmuş, C.; Çağlard, M.; Türüt A. The electrical modulus and other dielectric properties by the impedance spectroscopy of $LaCrO_3$ and $LaCr_{0.90}Ir_{0.10}O_3$ perovskites, *RSC Adv.* **2018**, vol. 8, nº 9, p. 4634-4648, doi: 10.1039/C7RA13261A.

TOC Graphic